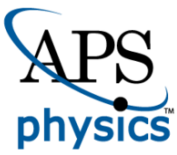

Heat transport in the anisotropic Kitaev spin liquid

Angelo Pidatella, Alexandros Metavitsiadis, and Wolfram Brenig

Phys. Rev. B **99**, 075141 — Published 20 February 2019

DOI: 10.1103/PhysRevB.99.075141

Heat transport in the anisotropic Kitaev spin liquid

Angelo Pidatella,[1,*] Alexandros Metavitsiadis,[2,†] and Wolfram Brenig[2,‡]

[1] *Institut für Theoretische Physik, Technische Universität Dresden, D-01062 Dresden, Germany*
[2] *Institut für Theoretische Physik, Technische Universität Braunschweig, D-38106 Braunschweig, Germany*

(Dated: February 1, 2019)

We present a study of longitudinal thermal transport in the Kitaev spin model on the honeycomb lattice, focusing on the role of anisotropic exchange to cover both, gapless and gapped phases. Employing a complementary combination of exact diagonalization on small systems and an average gauge configuration approach for up to $\sim O(10^4)$ spinful sites, we report results for the dynamical energy current auto-correlation function as well as the dc thermal conductivity over a wide range of temperatures and exchange anisotropies. Despite a pseudogap in the current correlation spectra, induced by emergent thermal gauge disorder on any finite system, we find that in the thermodynamic limit, gapless and gapful phases both feature normal dissipative transport, with a temperature dependence crossing over from power law to exponentially activated behavior upon gap opening.

I. INTRODUCTION

Quantum spin liquids (QSL) represent a rare form of magnetic matter, with fluctuations strong enough to suppress the formation of local order parameters even at zero temperature. QSLs typically result from frustration of magnetic exchange and tend to exhibit many peculiar properties, such as massive entanglement, quantum orders and fractionalized excitations [1, 2]. Among the many models proposed for putative QSLs, Kitaev's compass exchange Hamiltonian on the honeycomb lattice stands out as one of the few, in which a $\mathbb{Z}_2$ QSL can exactly be shown to exist [3]. In fact, pairs of spins in this model fractionalize in terms of mobile Majorana fermions coupled to static $\mathbb{Z}_2$ gauge fields [3–7]. Solid state realizations of Kitaev's model are based on Mott-insulators with strong spin-orbit coupling (SOC) [8–11], although residual non-Kitaev exchange interactions remain an issue at low temperatures and low energies, where most of the present systems still tend to order magnetically [12].

Mobile Majorana matter has been suggested to leave several fingerprints in spectroscopic measurements, like inelastic neutron [13–15], Raman scattering [16], as well as in local resonance probes [17, 18]. Apart from spectroscopy, thermal transport is yet another powerful tool, able to discriminate microscopic models of elementary excitations and their scattering mechanisms in quantum magnets - see Ref. [19] for a review. Among the candidates for Kitaev QSLs, α-$RuCl_3$ [20] has been under intense scrutiny regarding measurements of the longitudinal thermal conductivity κ [21–24]. At first, heat transport by itinerant spin excitations had been inferred from an anomaly in the in-plane longitudinal heat conductivity κ_{xx} at around 100 K [21], and from a magnetic field-induced low-temperature enhancement of κ_{xx} for fields $B \gtrsim 8$ T parallel to the material's honeycomb planes [22]. These interpretations however, have recently been ruled out by results for the out-of-plane heat conductivity κ_{zz} where both types of anomalies are present as well [23]. The emergent picture for rationalizing the *longitudinal* heat transport in α-$RuCl_3$ material is thus, that its most salient features can be explained by phononic heat transport which is likely to be renormalized by scattering from Majorana matter [23, 24]. However, it remains to be settled whether also a sub-leading direct magnetic contribution to the heat transport is present, masked by the phononic transport. Very recently also *transverse* thermal transport in magnetic fields, i.e. thermal Hall conductivity κ_{xy}, and its potential quantization has been observed in α-$RuCl_3$ [25]. This may be a rather strong evidence for Kitaev physics and chiral Majorana edge modes in this material. An alternative explanation of the thermal Hall effect in terms of chiral magnon edge states has been proposed [26, 27], which however, would not lead to quantization of κ_{xy}. Furthermore, spin-phonon coupling plays an important role for the understanding of the thermal Hall effect, and has recently been discussed in the literature [28, 29].

Theoretically, thermal transport studies in pure Kitaev QSLs have been performed using quantum Monte Carlo in 2D [30] or applying ED in 1D and 2D [31–33]. Thermal transport in Kitaev-Heisenberg ladders has been considered recently, employing ED and quantum typicality [34]. Magnetically *ordered* phases of a Kitaev-Heisenberg model have also been investigated for transport using spin wave calculations [35]. Remarkably, in the 2D QSL case, all of these studies have been confined to the point of C_3-symmetrically sized, isotropic compass exchange, i.e. the *gapless* phase of the Kitaev model. The main purpose of this work is to step beyond this limitation and investigate the longitudinal thermal conductivity, covering also anisotropic Kitaev exchange, ranging from the gapless to the gapped case. Exploring both phases, we find that regardless of the exchange coupling regime, the system supports a finite dc transport coefficient at all *non-zero* temperatures investigated, however with the emergence of thermal activation behavior in the gapped phase.

The outline of this paper is as follows: in Sec. II we briefly recall the properties of the Kitaev model, along with basic ingredients of thermal transport calculations,

as used in this work. In Sec. III we detail our results for the thermal conductivity versus the anisotropy of the exchange coupling, as obtained using the average gauge configurations (AGC). The method is explained in Sec. III A, which is then applied to study the dynamical heat current auto-correlation function in Sec. III B, and the dc heat conductivity in Sec. III C. We conclude in Sec. IV. Appendix A relates our findings to transport-phenomenology. Appendix B reports analytical results for the thermal conductivity in the uniform gauge field sector.

II. MODEL

We study the longitudinal dynamical thermal conductivity of the Kitaev model in the presence of *anisotropy*, introduced by tuning the relative exchange couplings and considering both, gapless and gapped regimes. The Hamiltonian is

$$\mathcal{H} = \sum_{\langle l,m\rangle,\lambda(\langle l,m\rangle)} J_\lambda \sigma_l^\lambda \sigma_m^\lambda \,, \tag{1}$$

where $\langle l,m\rangle$ indicates nearest-neighbors on a 2D honeycomb lattice (HL) of $2N$ sites, with J_λ and σ^λ the exchange couplings and the Pauli matrices, respectively, for coordinates $\lambda = x,y,z$, as shown in Fig. 1(a). Model (1) can be mapped onto a sum of 2^N Hamiltonians of non-interacting itinerant Majorana fermions, each of which is classified by a fixed, distinct distribution of values of N static $\mathbb{Z}_2$ gauge fields $\eta_{\mathbf{r}} = \pm 1$, residing on, e.g., the blue bonds in Fig. 1(a). The Majorana fermions of each gauge sector $\{\eta_{\mathbf{r}}\}$ can be rewritten in terms of N spinless non-interacting fermions $d_{\mathbf{r}}^{(\dagger)}$ with occupation numbers 0,1. This implies a total of 2^{2N} states of gauges and spinless fermions, consistent with the dimension of the original spin Hilbert space. Each of the 2^N fermionic sub-Hamiltonians is a QSL with spin correlations not exceeding nearest neighbor distance. Several routes have been documented to achieve the aforementioned mapping and we refer to Refs. [3–7] for details. In this $\eta_{\mathbf{r}}, d_{\mathbf{r}}^{(\dagger)}$-language (1) reads

$$\mathcal{H} = \sum_{\mathbf{r}} h(\mathbf{r}) = \sum_{\mathbf{r}} \Big[J_x (d_{\mathbf{r}}^\dagger + d_{\mathbf{r}})(d_{\mathbf{r}+\mathbf{e}_x}^\dagger - d_{\mathbf{r}+\mathbf{e}_x}) + J_y (d_{\mathbf{r}}^\dagger + d_{\mathbf{r}})(d_{\mathbf{r}+\mathbf{e}_y}^\dagger - d_{\mathbf{r}+\mathbf{e}_y}) + J_z \eta_{\mathbf{r}} (2 d_{\mathbf{r}}^\dagger d_{\mathbf{r}} - 1) \Big] \,. \tag{2}$$

Here, for convenience, the J_z-bonds, which feature only an $\eta_{\mathbf{r}}$-dependent on-bond potential for the fermions are shrunk onto just a point, transforming the HL into a square lattice (SL), with primitive vectors $\mathbf{e}_{x,y}$ as depicted in Fig. 1(b). We will refer the SL geometry throughout this paper. To quantify the *anisotropy* of the Kitaev exchange, we employ a parameter α, such that $J_x = J_y = \alpha$, and $J_z = 3 - 2\alpha$. Tuning α allows to keep the fermionic energy scale $(J_x{+}J_y{+}J_z)/3{=}1{\equiv}J$ constant, while accessing both, the gapless and the gapped regime of the zero temperature spectrum of (2), for $1 > \alpha > 0.75$ and $0.75 > \alpha > 0$, respectively [3].

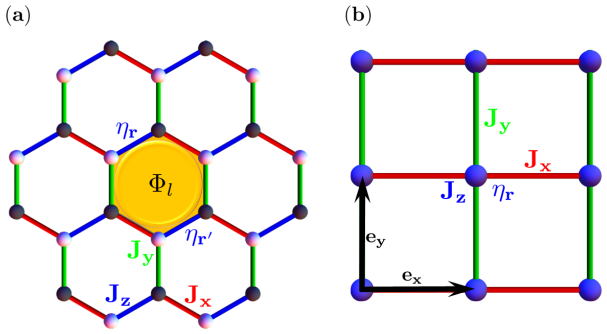

Figure 1. (a) Kitaev model on honeycomb lattice (HL). Red, green, blue colors label $J_{x,y,z}$ exchange interactions between black and white triangular sublattice sites. Yellow $\Phi_l = \eta_{\mathbf{r}}\eta_{\mathbf{r}'}$ refers to the flux, with gauge fields $\eta_{\mathbf{r}}, \eta_{\mathbf{r}'}$ attached to blue edge of the hexagon. (b) Kitaev model, shrunk onto square lattice (SL) of Eq. (2). $J_{x,y}$ (red, green edges) mediate fermion hopping/pairing, along lattice vectors $\mathbf{e}_{\mathbf{x},\mathbf{y}}$. Exchange interactions J_z and gauge fields $\eta_{\mathbf{r}}$ (blue vertices) set on-site energy.

Our discussion of the thermal conductivity is based on calculations within linear response theory, assuming the long wave length limit $\mathbf{q}{\to}0$. For this, thermal transport coefficients are computed from the energy current auto-correlation functions $\langle \mathcal{J}(t)\mathcal{J}\rangle$, where $\mathcal{J}$ is the energy current and $\langle \dots \rangle$ refers to the thermal trace [36]. The real part of thermal conductivity, i.e. $\kappa'(\omega)$, follows from the Fourier transform

$$C(\omega) = \frac{1}{N} \int dt e^{i\omega t} \langle \mathcal{J}(t)\mathcal{J}\rangle, \tag{3}$$

$$\kappa'(\omega) = \frac{\beta}{2\omega} \left(1 - e^{-\beta\omega}\right) C(\omega) \,. \tag{4}$$

Generically, $\kappa'(\omega) = 2\pi D\delta(\omega) + \kappa^{reg}(\omega)$. The *Drude* weight (DW) D refers to a ballistic channel, and if finite marks a perfect conductor. $\kappa^{reg}(\omega)$ encodes the dissipative parts of the heat flow. If $\kappa^{dc} = \kappa^{reg}(\omega \to 0)$ is finite, the system is a normal heat conductor with a finite DC conductivity. Interacting quantum systems with $D \neq 0$ are rare, see e.g. Ref. [36], and $D = 0$ for $N \to \infty$ has also been argued for the Kitaev model [32, 33]. In turn, a prime goal of this work will be the analysis of $\kappa^{reg}(\omega)$ and its limit for $\omega \to 0$ in order to determine the DC conductivity.

To derive the heat current operator in (3) one has to realize that most of the gauge sectors in (2) are not translationally invariant, due to the real space distribution of $\eta_{\mathbf{r}}$. In turn, we employ the polarization operator $\mathbf{P}$ [33], to obtain the current operator in real space

$$\mathbf{P} = \sum_{\mathbf{r}} \mathbf{r} h(\mathbf{r}), \quad \mathcal{J} = \frac{\partial \mathbf{P}}{\partial t} = i\,[\mathcal{H}, \mathbf{P}] \,. \tag{5}$$

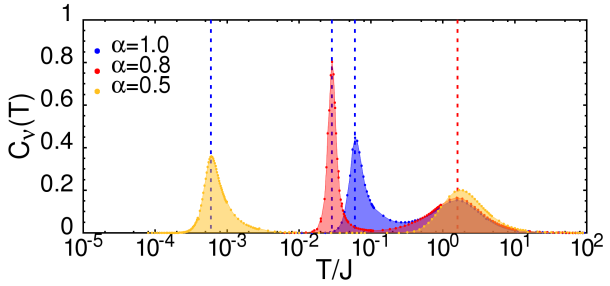

Figure 2. Specific heat $C_\nu(T)$ for $\alpha = 1.0, 0.8, 0.5$ from ED on N=6×6, i.e. 72 spinful sites versus T. Vertical lines at $T^\star_\alpha$ (blue dashed) and T_M (red dashed) indicate temperature scales for flux and fermion entropy release.

It is worth noting, that in a translationally invariant system $\mathcal{J}$ from (5) is exactly identical to that obtained from the continuity equation in the limit of $\mathbf{q}\to 0$. On the SL we get

$$\mathcal{J}_\mu = 2iJ_\mu \sum_{\mathbf{r}} [J_z \eta_{\mathbf{r}} \chi_{\mathbf{r}} \chi_{\mathbf{r}-\mathbf{e}_\mu} + \tau_\mu J_{\bar{\mu}} \chi_{\mathbf{r}} \chi_{\mathbf{r}+\mathbf{e}_x-\mathbf{e}_y}] \,, \quad (6)$$

with $\chi_{\mathbf{r}} = (d^\dagger_{\mathbf{r}} + d_{\mathbf{r}})$, $\bar{\mu} = y(x)$ and $\tau_\mu = +(-)$ for $\mu = x(y)$.

For the remainder of this work we resort to numerical methods to treat (3). For this we note, that not only the Hamiltonian, but also the current operator does not mediate transitions between gauge sectors. In turn, any thermal trace can be decomposed into a classical trace over gauges and a trace over the fermions, separately. For the latter, and for each fixed gauge sector $\{\eta\} = (\eta_1, \ldots, \eta_N)$, we define a $2N$ component spinor $\mathbf{D}^\dagger = (d^\dagger_1, \ldots, d^\dagger_N, d_1, \ldots, d_N)$ of the fermions, with indices $1 \ldots N$ referring to the sites on the SL. With this the Hamiltonian and the current for each gauge sector read $\mathcal{H} = \mathbf{D}^\dagger \mathbf{h}(\eta) \mathbf{D}$, and $\mathcal{J}_\mu = \mathbf{D}^\dagger \mathbf{j}_\mu(\eta) \mathbf{D}$. Using a Bogoliubov transformation U onto quasiparticle fermions $\mathbf{A}^\dagger = (a^\dagger_1, \ldots, a^\dagger_N, a_1, \ldots, a_N)$ via $\mathbf{A} = \mathbf{U}^\dagger \mathbf{D}$, the Hamiltonian is diagonalized as

$$\mathcal{H} = \sum_i \varepsilon_i(\{\eta\})(a^\dagger_i a_i - \frac{1}{2}), \quad (7)$$

with quasiparticle energies $\varepsilon_i(\{\eta\})$. The contribution of each gauge sector to (3) can then be obtained straightforwardly by a Wick-decomposition of $\langle \mathcal{J}(t)\mathcal{J} \rangle$ in the quasiparticle basis [32].

III. RESULTS

In this section we will present our results for the dynamical energy current auto-correlation function $C(\omega, T)$ and the dc-limit of the heat conductivity $\kappa^{dc}(T)$ versus anisotropy at finite temperatures.

A. Average gauge configuration method

Tracing over the gauge sectors in (3) can be done in various ways and to various degrees of precision. Among the methods are Markovian sampling of the gauges by QMC [30, 37], exact summation over all gauges, equivalent to ED of the spin model [32, 33], and summing only over a dominant subset of gauge configurations, i.e. the average gauge configuration (AGC) method [32, 33], which will be used here. The following sketches the main ideas of the AGC method, while for more details we refer the reader to Refs. [32, 33]. The notion of an average gauge configuration is trivial in the low- and the high-temperature limit. In the former, the gauges assume a flux-free configuration [3], and in the latter a typical gauge configuration is fully random. These limiting cases are separated by a temperature scale $T^\star_\alpha$ at which flux-proliferation occurs upon increasing temperature. Here α refers to the anisotropy parameter. $T^\star_\alpha$ scales with the energy to excite a single flux, i.e. the flux gap $\Delta_\Phi/J \ll 1$ [3]. Because of the latter inequality, $T^\star_\alpha$ and the crossover regime can be read off from the specific heat, i.e. from the entropy release of the gauge fields [37], since this is well separated from the fermionic energy scales $O(J)$. Our strategy will be to first determine $T^\star_\alpha$ and then to confine all evaluations of $C(\omega)$ to temperatures above this scale, such that averaging over only completely *random* gauge states is sufficiently justified for the gauge trace. Consequently, the remaining effective fermionic model is a binary disorder problem. It turns out that the temperature range accessible by this approach is large enough for our purposes.

To approximate $T^\star_\alpha$ we now calculate the specific heat $C_\nu(T) = T\partial S/\partial T$ [38]. This is done *exactly* on finite systems, tracing over both, fermions and gauges. The system sizes we can reach for this, namely $N \leq 6\times 6$, i.e. 72 spins, are larger than those for exact thermodynamics using the many body *spin basis*, however, still much smaller than those which will be used within the AGC subsequently. Fig. 2 shows the temperature dependence of the specific heat for three different values of anisotropy. As expected, two peaks develop at two different temperature scales, corresponding to the release of entropy from the gauge degrees of freedom and the mobile Majorana fermions, at $T^\star_\alpha$ and $T_M/J \sim 1$, respectively. Obviously, the global fermionic energy scale J is only weakly affected by the gauge disorder, and therefore the high-T peak remains rather insensitive to α. However the low-T peak at $T^\star_\alpha$ is strongly shifted to smaller temperatures, by roughly two orders of magnitude, upon decreasing α from 1 to 0.5. This finding is consistent with results from QMC [37]. While in principle $T^\star_\alpha$ sets an individual temperature scale for each α, above which averaging

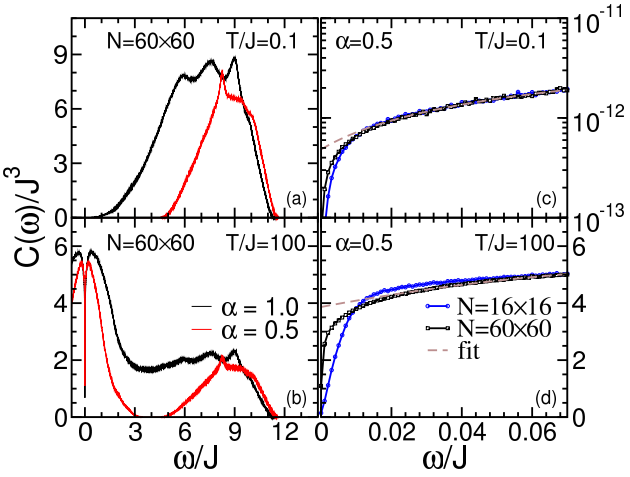

Figure 3. $C(\omega)$ from the AGC method, versus ω for two temperatures, $T/J = 0.1$ (a,c) and 100 (b,d). (a,b): Variation with anisotropy for $\alpha = 1, 0.5$ (black, red), corresponding to the gapless and gapful phase on a large ω-scale for N=60×60 sites. (c,d): Variation with system size N=16×16, 60×60 (blue, black) at low-ω for $\alpha = 0.5$. Brown dashed line: fitting-polynomial for $C(\omega, N$=60×60) to extract $\kappa^{dc}(T)$.

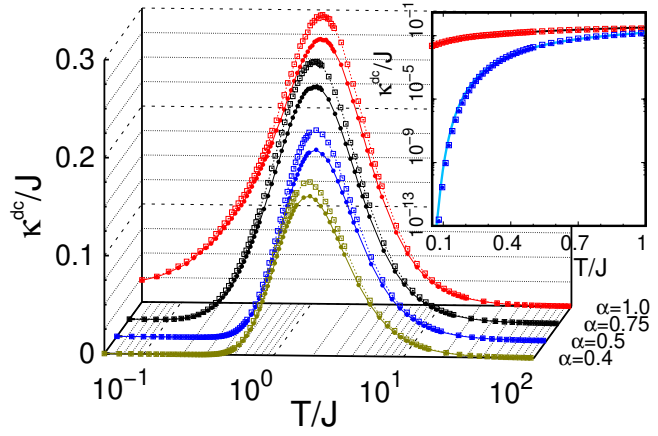

Figure 4. Thermal conductivity κ^{dc} versus T for various values of anisotropies $\alpha = 1.0 \ldots 0.4$, shown on the lower right axis, ranging from gapless to gapped phases. Two system sizes, N=16×16 (dashed with empty squares), and N=60×60 (solid with solid circles), are compared. Inset: low-T behavior for $\alpha = 1.0$ with red solid circles (red empty squares), and $\alpha = 0.5$ with blue solid circles (blue empty squares), for N=60×60(16×16). The data are superimposed onto two distinct fit functions T^{γ}, with γ=0.92 (black solid) and $e^{-\Delta/T}$, with Δ=2.30 (blue solid) for the gapless and the gapped cases respectively.

over fully random gauge configurations provides a sufficient approximation for the gauge trace, we will use the *maximum* of these, i.e. $T_{\alpha}^{\star,\max}/J \sim O(.1)$ as the lowest temperature to apply the AGC for all subsequent calculations, independent of α.

B. Dynamical current correlations

Now we turn to the dynamical current correlation function $C(\omega)$. Results on up to 60×60-sites systems are displayed in Fig. 3 for two representative anisotropy values $\alpha = 1.0(0.5)$. These place the system into the gapless(ful) phase. Two temperatures, i.e. T/J=0.1, 100 are shown, which allow to highlight the difference between low and high matter fermion densities. We begin with Fig. 3(a). Here the fermion occupation number at all momenta is small and the intensity is essentially due to two-fermion pair-breaking contributions to $C(\omega)$. For $\alpha = 0.5$, the one-particle dispersion displays a gap Δ, at $\Delta/J \approx 2$ [37], with a corresponding two-particle excitation gap ξ in $C(\omega)$ at $\xi/J \approx 4$. Moving to Fig. 3(b) the matter-fermion density is large and direct transport by thermally populated quasiparticle states contributes. In a clean system this transport would show up as a Drude peak strictly at ω=0. Due to the gauge disorder however, the Drude peak is smeared over a substantial range of finite frequencies $\sim O(J)$. Interestingly, the randomness provided for by the gauge field is not sufficient to fill in the gap completely, as is obvious from panel (a) and (b). Related observations have been made in Refs. [37, 39]. The 'smeared Drude peak' in Fig. 3(b) features a very narrow zero-frequency dip, which requires careful finite size analysis. Examples of such analysis are shown in Fig. 3(c,d) for the case of $\alpha = 0.5$. The main point can be read off best from panel (d), where it is amply clear, that as $N \to \infty$ the zero-frequency dip closes in onto the y-axis. This observation renders the system a normal, dissipative heat conductor in the thermodynamic limit and extends identical findings from Ref. [33] to the case of $\alpha \neq 1$. Note, that there is a difference of several orders of magnitude between $C(\omega)$ in Figs. 3(c) and 3(d). This is related to the thermal activation behavior in the gapful case, to be discussed in the next section.

C. DC-limit of heat conductivity

Based on a series of calculations as in Fig. 3, we have extrapolated the dc-limit $C(\omega \to 0, T, \alpha)$ over a wide range of T and α, sufficient to acquire a consistent picture of the thermal conductivity $\kappa^{dc}(T, \alpha)$ both, in the gapless and the gapful regime. This result is depicted in Fig. 4. To arrive at this, the brown dashed lines in Fig. 3(c,d) exemplarily indicate the extrapolation procedure performed, for each of the largest systems, i.e. for N=60×60. It consists of least-square fitting of the low-ω range of the correlation function for each pair of T, α by second order polynomials, from which the dc value $C(\omega \to 0, T)$ is extracted. We have chosen a range of $0.02 \leq \omega/J \leq 0.12$ to determine the coefficients of the polynomial in all cases. To obtain some form of finite-size

scaling, we have compiled the results of the fitting procedure for two system sizes, i.e. $N{=}L{\times}L$ and $L{=}\{16, 60\}$, into Fig. 4, showing dashed (solid) curves with empty squares (solid circles), for $L{=}16(60)$. Although the linear dimension of the systems shown differs by almost a factor of 4, κ^{dc} displays only minimal differences for most of the temperatures. Even for $T/J \approx 1$, where the absolute error between different system sizes becomes the largest [40], only a small, systematic correction towards lower values with increasing system size is observed for every α. This implies visible, but satisfyingly little finite-size effects, presumably putting the largest system sizes rather close to the thermodynamic limit.

Fig. 4 is a main result of this paper. It extends previous analysis of the thermal conductivity of the Kitaev model [30, 33] into the anisotropic regime. It demonstrates a qualitative change of the temperature dependence of $\kappa^{dc}(T, \alpha)$, as the system crosses over from the gapless to the gapful spectrum. In the former the thermal conductivity roughly scales with a power law, $\kappa^{dc} \sim T^{\gamma}$ for $T/J \ll 1$, while in the latter an exponential behavior with $\kappa^{dc} \sim \exp(-\Delta/T)$ provides a reasonable description. This is in line with the notion of quasiparticle transport, since the activation gap Δ is consistent with the one-particle gap, e.g. $\Delta/J \sim 2$ for $\alpha = 0.5$ as discussed in Sec. III B. For a comparison of the thermal transport properties in the absence of gauge excitations we refer the reader to App. B.

We would like to emphasize, that while the trend of the curves in Fig. 4 might suggest a strictly vanishing κ^{dc}, e.g. for $\alpha \geq 0.5$ and $T/J \lesssim 0.5$, this is *not* so, based on our results. Rather, the y-axis scale in Fig. 3(c) is very small, albeit finite. Such small orders of magnitude are consistent with the rapid low temperature suppression by the exponential activation. In turn, our findings suggest, that the Kitaev model is a normal dissipative heat conductor at all finite temperatures, at least above $T^{\star}_{\alpha}$, for all α.

IV. CONCLUSION

In summary, we have investigated the longitudinal dynamical thermal conductivity of the Kitaev model on the honeycomb lattice with anisotropic exchange couplings. Using an average gauge configuration method, combined with exact diagonalization of the matter fermion sector, systems of up 7200 spinful sites have been analyzed over a wide range of temperatures and anisotropies. We have confirmed both, the applicability and range of validity of our method by complementary exact analysis of thermodynamic properties. Our main finding is that for all temperatures and anisotropies investigated, the systems feature normal dissipative transport, consistent with scattering of the matter fermions from the static fluxes, and also consistent with a temperature dependence set by the matter fermion mass gap. From an experimental point of view, transport in putative Kitaev quantum spin liquids could be interesting under strain in order to tune exchange couplings, while monitoring the temperature dependence of thermal transport.

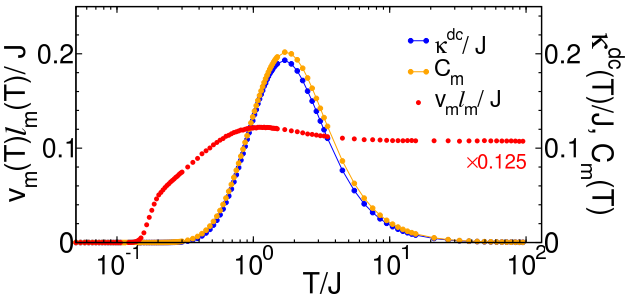

Figure 5. Red solid circles: $\kappa^{dc}(T)/C_m(T) \equiv v_m(T)\ell_m(T)$. versus T at $\alpha = 0.5$. Solid lines with solid circles: $\kappa^{dc}(T)$ (blue) and $C_m(T)$ (yellow) evaluated by AGC method on $N = 32 \times 32$ sites.

V. ACKNOWLEDGMENTS

We thank M. Vojta and C. Hess for comments and discussion. Work of A.P. and W.B. has been supported in part by the DFG through SFB 1143, project A02. Work of W.B. has been supported in part by QUANOMET and the NTH-School CiN. W.B. also acknowledges kind hospitality of the PSM, Dresden. This research was supported in part by the National Science Foundation under Grant No. NSF PHY-1748958.

Appendix A: Kinetic model of thermal conductivity

This appendix is a digression into phenomenology, which we add out of curiosity. It is customary to perform kinetic modeling of thermal conductivities, expressing $\kappa^{dc}(T)$ in terms of quasiparticle properties [19, 41]

$$\kappa^{dc}(T) \approx \sum_{k,p} C_{k,p}(T) v_{k,p}(T) \ell_{k,p}(T)\,, \tag{A.1}$$

where $C_{k,p}(T), v_{k,p}(T)$, and $\ell_{k,p}(T)$ refer to the specific heat, velocity, and mean free path at momentum k of quasiparticles of type 'p'. In the present case these types are fluxes, $p{=}f$, and matter fermions, $p{=}m$. Disentangling the contributions to $\kappa^{dc}(T)$ from various types 'p' is only an option, if their spectral supports are well separated. As one can read off directly from Fig. (2), exactly this is possible for strong anisotropy, e.g. $\alpha = 0.5$, where the flux peak in $C_{\nu}(T)$ at $T^{\star}_{\alpha}$ is well separated from the dominant contributions to the specific heat of the fermions. Moreover, realizing that the flux velocity $v_{k,f} = 0$, and adopting the usual approximation to drop the momentum summation in (A.1)

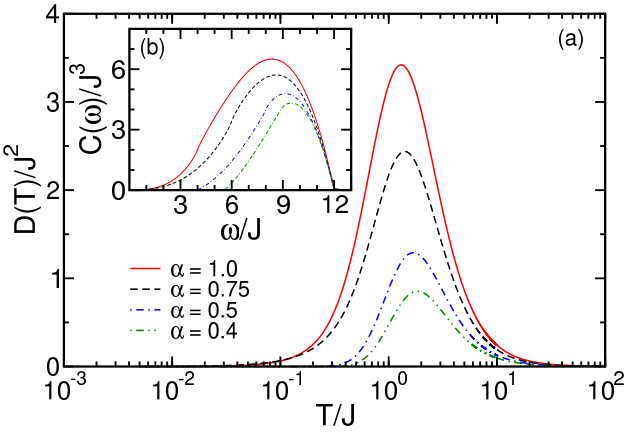

Figure 6. Results at uniform $\eta_{\mathbf{r}} = 1$, for various values of $\alpha = 1 \cdots 0.4$, ranging from gapless to gapful phases. (a) Drude weight D versus T. (b) Regular part of the dynamical current auto-correlation function $C(\omega)$ versus ω at $T = 0$.

in favor of momentum integrated quantities, one gets $\kappa^{dc}(T) \sim C_m(T)v_m(T)\ell_m(T)$ for $T > T^\star_\alpha$.

From this it is tempting to analyze the ratio of $\kappa^{dc}(T)/C_m(T)$, as obtained from our calculations, e.g. for $\alpha = 0.5$. This is shown in Fig. 5. It is this variation of $v_m(T)\ell_m(T)$ with T, which this appendix is meant to speculate on as follows. First, at all $T > T^\star_\alpha$, the flux lattice is completely random, setting a mean free path for the fermions, independent of T. Second, for sufficiently large T, fermions far up in the Dirac cone set the Fermi velocity, which is also independent of T. Third, upon lowering T, fermions close to the gap set $v_m(T)$. This velocity approaches zero as $T \to 0$. Remarkably, these points are roughly captured in the temperature variation of $v_m(T)\ell_m(T)$, seen in Fig. 5.

Appendix B: Uniform gauge state

In this appendix we present results for the thermal transport of the Kitaev model, discarding gauge excitations and assuming the ground state gauge $\eta_{\mathbf{r}} = 1$.

After Fourier and Bogoliubov transforming Eq. (2), the single particle dispersion Eq. (7) reads $\varepsilon_{\mathbf{k}} = 2[(J_z - \mathcal{C}_{\mathbf{k}})^2 + \mathcal{S}^2_{\mathbf{k}}]^{1/2}$ with

$$\mathcal{C}_{\mathbf{k}} = \sum_{\mu=x,y} J_\mu \cos k_\mu \ , \quad \mathcal{S}_{\mathbf{k}} = \sum_{\mu=x,y} J_\mu \sin k_\mu \ .$$

Similarly, the current operator in Eq. (6) acquires a simple expression in momentum space yielding the correlation function

$$C_{\mu\mu}(\omega) = \frac{2\pi}{N} \sum_{\mathbf{k}} \{2|l_{\mathbf{k},\mu}|^2 [2f_{\mathbf{k}}(1-f_{\mathbf{k}})\delta(\omega) + f^2_{\mathbf{k}}\delta(\omega + 2\varepsilon_{\mathbf{k}}) + (1-f_{\mathbf{k}})^2\delta(\omega - 2\varepsilon_{\mathbf{k}})]\} \ , \quad \text{(B.1)}$$

with $2l_{\mathbf{k},\mu} = \varepsilon_{\mathbf{k}}\partial\varepsilon_{\mathbf{k}}/\partial k_\mu$, and $f_{\mathbf{k}} = 1/(e^{\beta\varepsilon_{\mathbf{k}}}+1)$ the Fermi function. In (B.1), the term $\sim \delta(\omega)$ refers to the Drude weight, i.e. the ballistic dc channel, while the rest refers to finite-ω contributions from pair-breaking terms. We refer to Ref. [33] for further details.

Fig. 6(a) depicts the temperature dependence of the Drude weight, for several values of $\alpha = 1 \ldots 0.4$, ranging from gapless to gapful phases. We fix $\mu\mu = xx$ and drop these indices. At any $T > 0$, $D(T)$ is finite in the gapless (gapful) regime, with $D \sim T^2 (\sim \exp(-\Delta/T))$ at $T/J \ll 1$, and Δ being the one-particle gap of matter excitations. This implies, that within the uniform gauge field sector, the system is a ballistic conductor at $T > 0$. The overall temperature dependence of D is somewhat similar to that of $\kappa^{dc}(T)$ in Fig. 4. Only at $\alpha = 0.75$, the former exhibits a polynomial onset, while the latter shows an exponential one. This is due to the renormalization of the boundary between gapless and gapped phases by gauge excitations [37]. Fig. 6(b) shows $C(\omega{>}0)$ at $T = 0$. It is similar to the frequency dependence of the *low* temperature $C(\omega)$ evaluated via the AGC method, Fig. 3(a). $C(\omega, T = 0)$ displays a low-frequency power-law behavior in the gapless cases, and a linear onset above the gap for the gapful ones.

* angelo.pidatella@tu-dresden.de
† a.metavitsiadis@tu-bs.de
‡ w.brenig@tu-bs.de

[1] L. Balents, Nature **464**, 199-208 (2010).
[2] L. Savary and L. Balents, Rep. Prog. Phys. **80**, 016502 (2017).
[3] A. Kitaev, Ann. Phys. (N.Y.) **321**, 2 (2006).
[4] X.-Y. Feng, G.-M. Zhang, and T. Xiang, Phys. Rev. Lett. **98**, 087204 (2007).
[5] H.-D. Chen and Z. Nussinov, J. Phys. A: Math. Theor. **41**, 075001 (2008).
[6] Z. Nussinov and G. Ortiz, Phys. Rev. B **79**, 214440 (2009).
[7] S. Mandal, R. Shankar and G. Baskaran, J. Phys. A: Math. Theor. **45**, 335304 (2012).
[8] G. Khaliullin, Prog. Theor. Phys. Suppl. **160**, 155 (2005).
[9] G. Jackeli and G. Khaliullin, Phys. Rev. Lett. **102**, 017205 (2009).
[10] J. Chaloupka, G. Jackeli, and G. Khaliullin Phys. Rev. Lett. **105** 027204 (2010).
[11] Z. Nussinov and J. van den Brink, Rev. Mod. Phys. **87**, 1 (2015).
[12] S. Trebst, *arXiv:1701.07056.*
[13] A. Banerjee, C. A. Bridges, J. Q. Yan, A. A. Aczel, L. Li, M. B. Stone, G. E. Granroth, M. D. Lumsden, Y. Yiu, J. Knolle, S. Bhattacharjee, D. L. Kovrizhin, R. Moessner, D. A. Tennant, D. G. Mandrus, and S. E. Nagler, Nat. Mater. **15**, 733 (2016).
[14] A. Banerjee, J. Yan, J. Knolle, C. A. Bridges, M. B. Stone, M. D. Lumsden, D. G. Mandrus, D. A. Tennant, R. Moessner, and S. E. Nagler, Science **356**, 6342 (2017).
[15] A. Banerjee, P. Lampen-Kelley, J. Knolle, C. Balz, A.

A. Aczel, B. Winn, Y. Liu, D. Pajerowski, J. Yan, C. A. Bridges, A. T. Savici, B. C. Chakoumakos, M. D. Lumsden, D. A. Tennant, R. Moessner, D. G. Mandrus, and S. E. Nagler, Nat. Part. J. Quantum Mater. **3**, 8 (2018).

[16] J. Knolle, G.W. Chern, D.L. Kovrizhin, R. Moessner, and N.B. Perkins, Phys. Rev. Lett. **113**, 187201 (2014).

[17] S.-H. Baek, S.-H. Do, K. Y. Choi, Y.S. Kwon, A.U.B. Wolter, S. Nishimoto, J. van den Brink, and B. Büchner, Phys. Rev. Lett. **119**, 037201 (2017).

[18] J. Zheng, K. Ran, T. Li, J. Wang, P. Wang, B. Liu, Z.-X. Liu, B. Normand, J. Wen, and W. Yu, Phys. Rev. Lett. **119**, 227208 (2017).

[19] C. Hess, *arXiv:1805.01746*.

[20] K. W. Plumb, J. P. Clancy, L. J. Sandilands, V. V. Shankar, Y. F. Hu, K. S. Burch, H.-Y. Kee, and Y.-J. Kim, Phys. Rev. B **90**, 041112 (2014).

[21] D. Hirobe, M. Sato, Y. Shiomi, H. Tanaka, E. Saitoh, Phys. Rev. B **95**, 241112 (2017).

[22] I.A. Leahy, C.A. Pocs, P.E. Siegfried, D. Graf, S.-H. Do, K.-Y. Choi, B. Normand, and M. Lee, Phys. Rev. Lett. **118**, 187203 (2017).

[23] R. Hentrich, A. U. B. Wolter, X. Zotos, W. Brenig, D. Nowak, A. Isaeva, T. Doert, A. Banerjee, P. Lampen-Kelley, D. G. Mandrus, S. E. Nagler, J. Sears, Y.-J. Kim, B. Büchner, C. Hess, Phys. Rev. Lett. **120**, 117204 (2018).

[24] Y. J. Yu, Y. Xu, K. J. Ran, J. M. Ni, Y. Y. Huang, J. H. Wang, J. S. Wen, and A. Y. Li, Phys. Rev. Lett. **120**, 067202 (2018).

[25] Y. Kasahara, T. Ohnishi, Y. Mizukami, O. Tanaka, S. Ma, K. Sugii, N. Kurita, H. Tanaka, J. Nasu, Y. Motome, T. Shibauchi, and Y. Matsuda, Nature **559**, 227-231 (2018).

[26] J. Cookmeyer, and J. E. Moore, Phys. Rev. B **98**, 060412(R) (2018).

[27] P. A. McClarty, X. -Y. Dong, M. Gohlke, J. G. Rau, F. Pollmann, R. Moessner, and K. Penc, Phys. Rev. B **98**, 060404(R) (2018).

[28] M. Ye, G. B. Halász, L. Savary, and L. Balents, Phys. Rev. Lett. **121**, 147201 (2018).

[29] Y. Vinkler-Aviv, and A. Rosch, Phys. Rev. X **8**, 031032 (2018).

[30] J. Nasu, J. Yoshitake, and Y. Motome, Phys. Rev. Lett. **119**, 127204 (2017).

[31] R. Steinigeweg and W. Brenig, Phys. Rev. B **93**, 214425 (2016).

[32] A. Metavitsiadis and W. Brenig, Phys. Rev. B **96**, 041115(R) (2017).

[33] A. Metavitsiadis, A. Pidatella, and W. Brenig, Phys. Rev. B **96**, 205121 (2017).

[34] A. Metavitsiadis, C. Psaroudaki, and W. Brenig, *arXiv:1806.02344*.

[35] G. L. Stamokostas, P. E. Lapas, and G. A. Fiete, Phys. Rev. B **95**, 064410 (2017).

[36] F. Heidrich-Meisner, A. Honecker, and W. Brenig, Eur. Phys. J. Special Topics **151**, 135 (2007).

[37] J. Nasu, M. Udagawa, and Y. Motome, Phys. Rev. B **92**, 115122 (2015).

[38] The specific heat is evaluated numerically via temperature derivative of entropy

$$S(T) = \frac{1}{T}(\langle E_m(T)\rangle - F(T)) \qquad \text{(B.2)}$$

$E_m = \sum_i (\varepsilon_i^\eta - \frac{1}{2}) a_i^\dagger a_i$ is the thermal energy of the matter fermions in a particular $\{\eta\}$ configuration, with ε_i the single-particle energy, and $F(T)=-T\ln Z$ the free energy of the matter fermions. Here $Z = Tr_{\{\eta\}} Tr_{\{a(\eta)\}} e^{-\beta\mathcal{H}}$ is the total partition function.

[39] J. Nasu, and Y. Motome, Phys. Conf. Ser. **683**, 012037 (2016).

[40] The relative error $|\kappa_{60}^{dc}(T) - \kappa_{16}^{dc}(T)|/\kappa_{60}^{dc}(T)$ between the systems sizes $L = 16$ and 60, remains of $O(10\%)$ for the temperatures considered in Fig. 4.

[41] C. Hess, C. Baumann, U. Ammerahl, B. Büchner, F. Heidrich-Meisner, W. Brenig, and A. Revcolevschi, Phys. Rev. B **64**, 184305 (2001).